**SIRM 2015 – 11th International Conference on Vibrations in Rotating Machines,
Magdeburg, Deutschland, 23. – 25. February 2015**

Oil Flow in Connecting Channels of Floating Ring Bearings

Rob Eling [1,2], **Ron van Ostayen** [2], **Daniel Rixen** [3]

[1] Research and Development, Mitsubishi Turbocharger, 1332EC, Almere, The Netherlands, reling@mtee.eu
[2] Precision and Microsystems Engineering, Delft University of Technology, 2628CD, Delft, The Netherlands
[3] Institute of Applied Mechanics, Technische Universität München, 85748, Garching, Germany

Abstract

Floating ring bearings contain an inner and an outer fluid film, interconnected by oil connecting channels. These channels allow oil to flow from the outer film to the inner film. The channels are similar to lid-driven cavities and vortices exist in these channels. In addition, due to the shear-driven flow, sharp pressure gradients exist at the inlet and outlet edges of these channels. In order to include the presence of these channels in a computationally efficient Reynolds-based model, a channel flow model is developed, based on multivariate regression analysis applied to the results of a CFD-model of a single oil connecting channel. Results show that at eccentricites below 0.3, the oil connecting channels have a significant influence on the pressure distribution in the floating ring bearing, which is captured by the proposed channel flow model.

Nomenclature

C	Bearing clearance [m]	s	Shaft (subscript)
D	Bearing diameter [m]	T	Torque [N.m]
h	Film thickness [m]	U	Wall velocity [m/s]
I	Moment of inertia [kg.m^2]	ε	Eccentricity ratio [-]
L	Bearing length [m]	η	Viscosity [Pa.s]
p	Pressure [Pa]	θ	Circumferential coordinate [rad]
Q	Mass flow [kg/s]	ρ	Fluid density [kg/m^3]
r	Ring (subscript)	Ω	Rotation speed [rad/s]

1 Introduction

Floating ring bearings are often used in automotive turbochargers. The function of floating ring bearings (FRBs) is to optimally support radial shaft loads, that is, to enable free shaft rotation with minimal friction losses, negligible wear and low audible noise output. The FRB is a type of hydrodynamic bearing which consists of a freely rotating intermediate ring in between the shaft and the bearing housing (see Figure 1). The FRB is fed with externally pressurized oil which flows through the outer and inner oil films and exits at the axial ends of the bearing. The rotation speed of the shaft and the ring relative to their counter faces results in hydrodynamic pressure buildup in the inner and outer oil films, which creates the carrying capacity of the FRB [1]. Evaluation of FRB critical performance criteria, such as friction losses and forced unbalance response, is often done using time-transient simulation due to the highly non-linear characteristics of the FRBs. Accurate FRB pressure distribution predictions are a key element in these simulations, as described in the literature review of Tian [2].

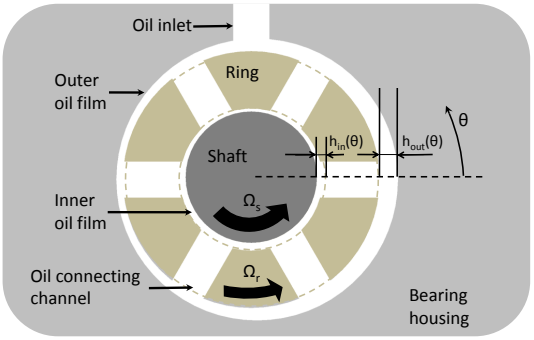

Figure 1: Schematic layout of a floating ring bearing.

Analytical approaches to predict the pressure distribution in a FRB are usually based on the assumption that the bearing is infinitely short (i.e. $\frac{L}{D} \to 0$) or infinitely long (i.e. $\frac{L}{D} \to \infty$) so that the Reynolds equation for fluid flow can be solved analytically, as has been done by several researchers (e.g. [3, 4, 5]). These computationally inexpensive analytical models can be used for analytical stability evaluation of a rotor-bearing system. However, the influence of complex geometries in the bearing, such as the oil connecting channels and the oil supply, can not be taken into account by these analytical methods. This also holds for the influence of spatial viscosity variation. Moreover, the assumption of an infinitely short bearing, neglecting the flow in circumferential direction, or an infinitely long bearing, neglecting the flow in axial direction, is generally not valid for most FRBs used in practice. As a result, pressure predictions based on analytical methods often have a limited validity, especially at higher bearing eccentricities.

Another approach to model the pressure distribution in a FRB is to use numerical discretization methods. Commonly, these methods solve the Reynolds equation by spatial discretization using finite element or finite difference schemes. When the discretization error is taken care of, this approach gives more accurate pressure predictions for the thin film areas of a FRB and can be extended to include thermal modeling, cavitation and non-Newtonian fluid behavior, see for example the thermohydrodynamic models of San Andrés [7] and Porzig [9]. The Reynolds equation in general, however, can only be used to predict the fluid flow in thin film areas and can not straightforwardly be used to predict the pressure in the oil connecting channels.

Some previous numerically-based studies on FRB dynamics [1, 6, 7] have ignored the presence of these oil connecting channels, whereas other studies [8, 9, 10] have modeled these channels as a pressure communication boundary condition, where the inner film pressure is equalized with the outer film pressure.

As the area of the oil connecting channels in some turbocharger applications accounts for over a quarter of the thin film area (see Figure 1), it seems inappropriate to neglect their influence on the pressure distribution of the FRB. Also the approach of modeling the oil connecting channels as pressure equalizers without any internal fluid dynamics seems inappropriate. These channels, namely, can be seen as two-sided lid-driven cavities, which are known to exhibit complex vortices in the fluid which influence the pressure distribution in the oil channel [11].

In this study, the influence of the FRB oil connecting channels is studied in more detail. Therefore, the following steps will be made:

1. Construction of a steady state 3D CFD model of the complete FRB to show the influence of the oil connecting channels on the total FRB pressure distribution and ring speed ratio.

2. Reducing the previous model to a steady state 2D CFD model on the axial midplane of a single oil connecting channel. This is done to get a better understanding of the input-output relations in the channel, see next step.
3. Using the steady state 2D CFD model, perturbations around the operating conditions are performed. Regression analysis is applied to the results, so a single oil connecting channel can be replaced by a flow function.
4. The flow function can then be used to replace the channels in the FRB model. In this case, we use the flow function to construct a computationally inexpensive 1D Reynolds model, which we compare with a 2D CFD model which does include the oil connecting channels.

Thus, the purpose of this study is to investigate if a computationally inexpensive Reynolds model with flow functions can give similar results to a CFD model, so that time-transient simulations of the FRB including the effect of the oil connecting channels is feasible.

2 FRB pressure distribution based on a 3D CFD model

2.1 3D CFD model details

First, a 3D steady state CFD FRB model was developed, see Figure 2, using a commercial FEM package [12]. The purpose of the model is to gain a detailed understanding of the flow in the oil connecting channels and its effect on the flow in the thin films.

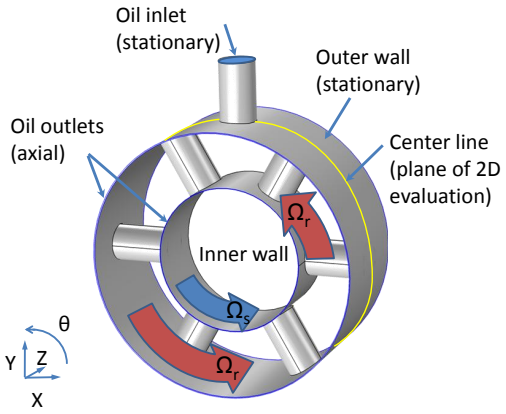

Figure 2: Fluid domain and boundary conditions of the FRB CFD model.

In this model, the shaft and ring eccentricties are prescribed. Thus, the film height functions are given by:

$$\begin{aligned} h_{out}(\theta) &= C_{out}(1 - \varepsilon_{r,x}\cos(\theta) - \varepsilon_{r,y}\sin(\theta)) \\ h_{in}(\theta) &= C_{in}(1 - \varepsilon_{s,x}\cos(\theta) - \varepsilon_{s,y}\sin(\theta)) + C_{out}(\varepsilon_{r,x}\cos(\theta) + \varepsilon_{r,y}\sin(\theta)) \end{aligned} \tag{1}$$

Shaft speed Ω_s is imposed as a velocity along the inner wall; ring speed Ω_r is imposed along the walls of the ring, see Figure 2. The fluid is modeled as an incompressible, isoviscous fluid. A supply pressure is imposed on the oil inlet. Axial outflow at the sides of the bearing occurs at ambient pressure. Axial symmetry is used to reduce the computational effort, based on the assumption that the ring and shaft do not tilt and thus are aligned with the bearing housing. Numerical values of a typical automotive turbocharger FRB are used, summarized in Table 1.

Oil inlet pressure $[Pa]$	$5 \cdot 10^5$	Oil viscosity $[Pa \cdot s]$	0.1
Outer ring radius $[m]$	$5 \cdot 10^{-3}$	Inner ring radius $[m]$	$3 \cdot 10^{-3}$
Outer ring width $[m]$	$5 \cdot 10^{-3}$	Inner ring width $[m]$	$4.75 \cdot 10^{-3}$
Outer clearance $[m]$	$50 \cdot 10^{-6}$	Inner clearance $[m]$	$20 \cdot 10^{-6}$
Oil channel radius $[m]$	$0.75 \cdot 10^{-3}$	Ring speed ratio $[-]$	0.25

Table 1: Properties of the reference rotor-bearing system

In order to maintain a reasonable element aspect ratio, the CFD model needs a large number of elements to describe the thin film sections. A mesh convergence study has been performed, which showed that a mesh of minimally $1 \cdot 10^6$ elements is suitable for this analysis. The Reynolds numbers for the films in this study are always lower than 100, hence, the fluid flow can be considered to be fully laminar. The Reynolds number for the oil connecting holes are typically between 100 and 2500, depending on the rotation speed, the channel geometry and the oil viscosity. In this study, cavitation is treated by setting negative pressures to zero.

2.2 3D CFD model results

A stationary study has been performed on the FRB 3D CFD model. Figure 3 shows the pressure distribution on the center line of the FRB in center position (zero eccentricity) at medium speed. As can be seen, the shear-driven flow of the films creates ram-pressure peaks at the edges of the oil connecting channels. This effect is mostly seen in the inner film, as the inner film thickness is smaller and also the relative wall velocity is higher than in the outer film. Figure 4 shows the circumferential pressure profiles at the center line of the oil films of the FRB in centric

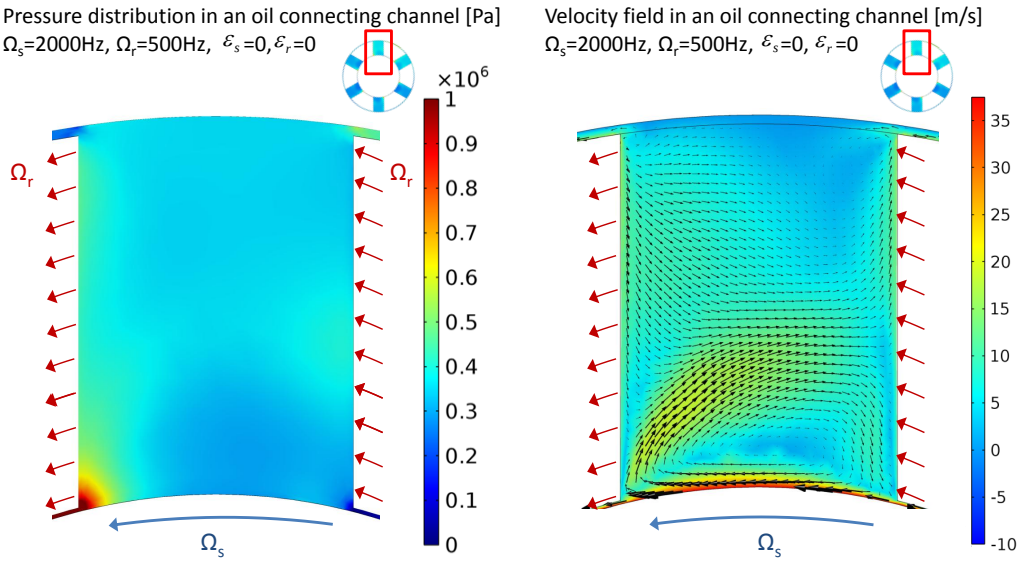

Figure 3: Center line pressure distribution (left) and oil flow in the connecting channel of the FRB with zero eccentricity, showing vortices and ram-pressure peaks caused by the shear flow of the inner and outer film.

and eccentric operation, where the supply pressure is situated around $\theta = \pi/2$. The influence of the oil connecting channels is clearly noticeable in sharp pressure gradients at the edges of the channel. In centric operation, peak pressures of $10^6 Pa$ in the inner film are observed. The peak pressures in the outer film are an order of magnitude smaller. Furthermore, it can be seen that the overall pressure in the inner fluid film is lower than the outer fluid film pressure due to the centrifugal forces on the fluid. The peak pressures of the fluid entering and exiting the channel were found to be well described by the approximation of Heckelman et.al. [13]:

$$\Delta P = C_1 \frac{\mu U}{h} + C_2 \rho U^2 \tag{2}$$

where C_1 and C_2 are constants depending on the channel geometry, and U is the relative velocity of the wall with respect to the ring.

At small eccentricities, the effect of the oil connecting channels still dominates the center line pressure distribution, as can be seen on the right hand side of figure 4. It was found that at higher eccentricity, the influence of the oil connecting channels decreases with respect to the influence of the hydrodynamic pressure buildup. In addition, the influence of the oil connecting channels on the pressure distribution decreases for lower viscosity.

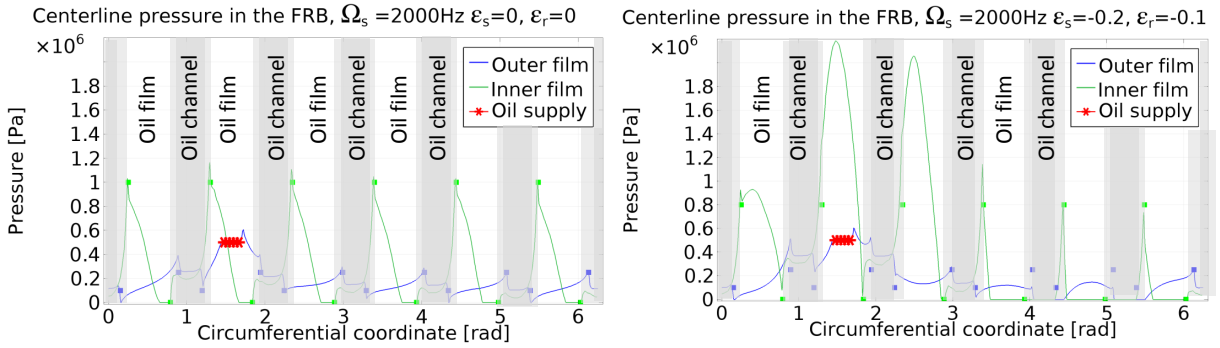

Figure 4: Center line pressure around the circumference of the oil films of the FRB at centric (left) and eccentric operation (right) clearly showing the influence of the oil connecting channels on the pressure distribution. The bullets in the graph represent the location of the boundary between the thin film and the connecting channel.

The ring can translate and rotate, depending on the load exerted by the fluid surrounding the ring. In order to determine the ring rotation speed, an often used approach [1, 2, 6, 9] has been to balance the drag torques created by the inner and outer oil film:

$$I_{ring}\ddot{\theta}_{ring} = \mathrm{T}_{inner} + \mathrm{T}_{outer} \tag{3}$$

where the drag torques of the films are determined by integrating the shear stress of the fluid over the inner and outer bearing areas. As can be seen in Figure 3, in addition to the shear force in the thin film areas, the fluid exerts a pressure on the side walls of the oil connecting channels. This pressure causes an additional torque which can drive the ring: $\mathrm{T}_{channel}$. Balancing the three torque terms, the ring speed ratio can be determined iteratively. The resulting ring speed ratios and the contributions in torque from both films as well as from the oil connecting channels are given in figure 5.

The pressure in the oil connecting holes appears to have a significant influence in determining the ring speed ratio: it delivers extra driving torque to the ring. As a result, the ring speed ratio is underestimated by up to 10% when the effect of the pressure inside the oil connecting channels is neglected. Under lower viscosity conditions, $\eta = 0.01[Pa \cdot s]$, the underestimation of ring speed ratio was smaller: $4 - 7\%$. This result was also found in the experiments of Trippett and Li [14], where the number of oil connecting channels was found to influence the ring speed ratio.

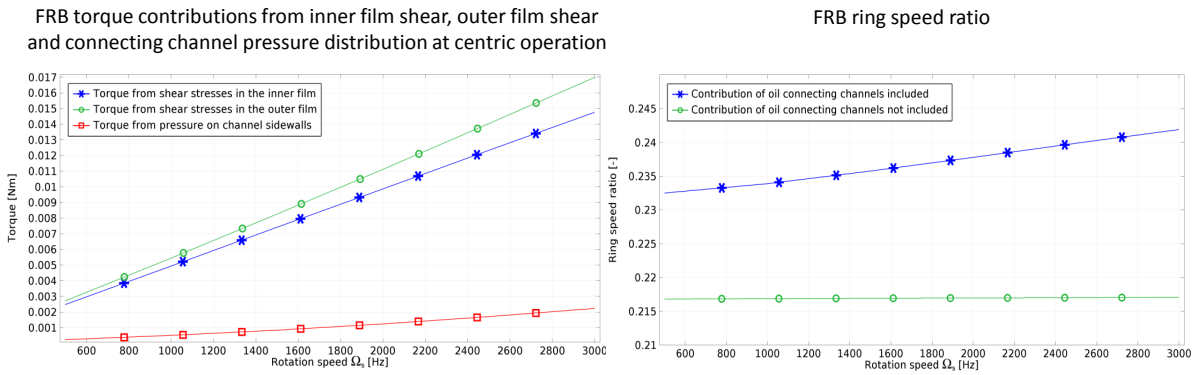

Figure 5: Torque contribution of the oil connecting channels (left) and its effect on the ring speed ratio (right). Although the torque contribution from the oil connecting channels is an order of magnitude smaller than the torques generated in the thin films; the ring speed ratio is significantly increased by it.

3 Channel flow functions based on a 2D channel cross-section

The results from the 3D CFD model show that the flow in the connecting channels influences the FRB pressure distribution and the ring speed ratio, and can therefore not be neglected. The FRB model is intended to be used for time-transient simulation in further studies, and therefore the use of a Navier-Stokes-based CFD model is too computationally expensive. Hence, a Reynolds-based model will be developed now, where the connecting channels will be replaced with flow functions. We will demonstrate this by performing 2D CFD simulations to study the flow in the center line plane. This method, however, can be extended to include the flow in axial direction.

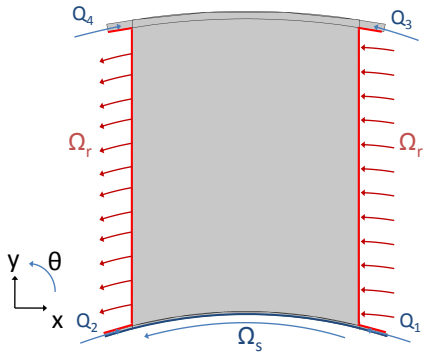

Figure 6: Base model for establishing the flow function model for the oil connecting channel. The velocities on the inner shaft and cavity side walls are imposed as well as the film pressures $(P_1...P_4)$ on the boundary of the channel. The resulting flows $(Q_1...Q_4)$ were evaluated using a CFD solver.

Considering a single oil channel as given in Figure 6, the flow through the channel boundaries $\{Q_1...Q_4\}$ can be approximated as a linearization around operating condition $\mathbf{P} = \mathbf{P}_0, \Omega = \Omega_0$:

$$\mathbf{Q} = \mathbf{Q}_0 + \mathbf{A}(\mathbf{P} - \mathbf{P}_0) + \mathbf{B}(\Omega - \Omega_0) \tag{4}$$

Where the flow $\mathbf{Q}_0$ is determined using a CFD evaluation at the operating condition. The coefficients of $\mathbf{A}$ and $\mathbf{B}$ are determined using multivariate regression analysis of CFD results around the operating point, see figure 7.

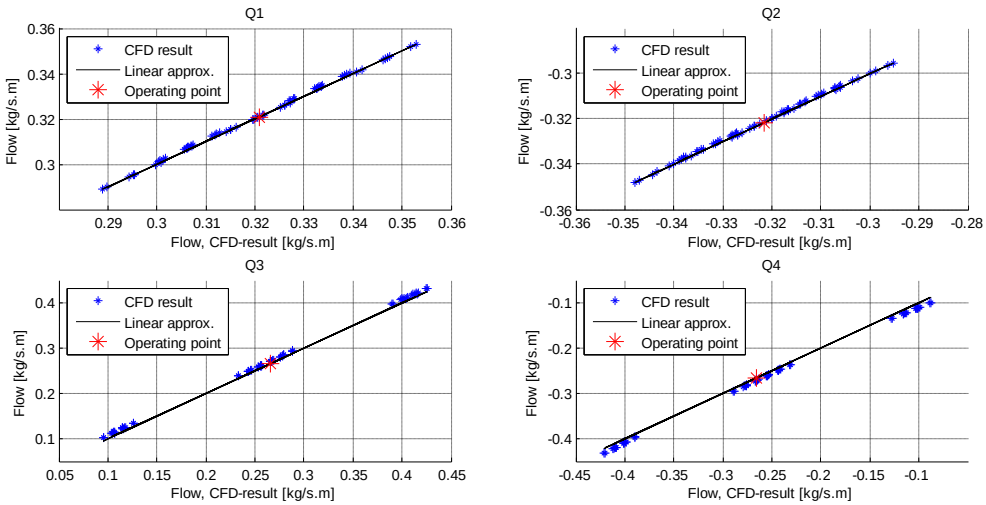

Figure 7: Linearization results of flow around operating point $\Omega_{s,o} = 10000rad/s, \Omega_{r,o} = 2500rad/s, \varepsilon_s = \varepsilon_r = 0$, using $\Delta P = 1e5Pa$ and $\Delta\Omega = 100rad/s$, $h_{in} = 20\mu m$, $h_{out} = 50\mu m$.

3.1 Flow function based on a 2D channel cross-section

Due to the curvature of the bearing and the difference in nominal film height, the matrices $\mathbf{A}$ and $\mathbf{B}$ are not symmetric. Their columnwise sums are zero, meaning conservation of mass holds. The flow approximation over the given range is equal to the CFD result within 1%. It was found that the dominant non-linearity originates from the dependency of flows Q3 and Q4 on rotation speeds Ω_s and Ω_r. In case the bearing operates in eccentric condition, the film thicknesses of the films surrounding the oil channel will deviate from their nominal values. It was found that a correction to the nominal flow $\mathbf{Q}_0$ is sufficient to correct for this; the pressure- and flow-dependent factors of $\mathbf{A}$ and $\mathbf{B}$ found under centric conditions can be used. Hence, the flow through the channel boundaries $\{Q_1, Q_4\}$ can be approximated as:

$$\mathbf{Q}(\varepsilon_s,\varepsilon_r) = \mathbf{Q}_0(\varepsilon_s,\varepsilon_r) + \mathbf{A}(\mathbf{P} - \mathbf{P}_0) + \mathbf{B}(\Omega - \Omega_0) \tag{5}$$

3.2 Flow function based on a 2D channel cross-section

The oil in the connecting channel exerts a pressure on the shaft, and is therefore a direct contributor to the FRB carrying capacity. As can be seen in figure 4, the pressure in the channel is mostly homogeneous, and therefore an equal pressure is assumed to act on the shaft over the channel area. In addition, due to the ring rotation speed, there is a centrifugal pressure difference between the inner and the outer fluid film:

$$\Delta P_{cent} = \frac{\rho {\Omega_r}^2 ({R_{out}}^2 - {R_{in}}^2)}{2} \tag{6}$$

The average pressure in the channel as a function of operating conditions is determined in a series of CFD simulations, and evaluated by a regression analysis, resulting in:

$$P_{channel}(\varepsilon_s,\varepsilon_r) = P_{channel,0}(\varepsilon_s,\varepsilon_r) + \mathbf{C}(\mathbf{P} - \mathbf{P}_0) + \mathbf{D}(\Omega - \Omega_0) \tag{7}$$

The pressure in the connecting channel at the location of film is corrected by the centrifugal pressure difference. The predicted channel pressures are similar to the CFD results within 1% within the tested range.

$$\begin{aligned} P_{channel,in} &= P_{channel} - \tfrac{\Delta P_{cent}}{2} \\ P_{channel,out} &= P_{channel} + \tfrac{\Delta P_{cent}}{2} \end{aligned} \tag{8}$$

Figure 8 gives the resulting linear approximation expressed in equation 7.

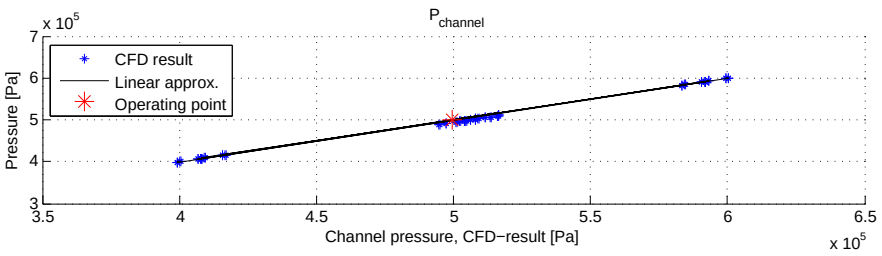

Figure 8: Average pressure in the connecting channel: CFD results and linearized predictions, using $\Delta P = 1e5Pa$ and $\Delta\Omega = 100rad/s$, $h_{in} = 20\mu m$, $h_{out} = 50\mu m$.

3.3 Torque contribution based on a 2D channel cross-section

As stated in section 2.2, the pressure distribution in the channel causes a net contribution of torque driving the ring in its rotation direction. This additional torque is evaluated in the 2D CFD channel setup depicted in figure 6 by integrating the pressure and shear forces over the channel walls. Analogous to the flow functions, this was done by linearization around an operating point:

$$T(\varepsilon_s,\varepsilon_r) = T_0(\varepsilon_s,\varepsilon_r) + \mathbf{E}^T(\mathbf{P}-\mathbf{P}_0) + \mathbf{F}^T(\Omega-\Omega_0) \tag{9}$$

Figure 9 shows the results of linearization of the torque around the operating point. The linearized prediction was equal to the CFD results within 2% over the evaluated range. The torque mostly depends on the ring and shaft rotation speeds.

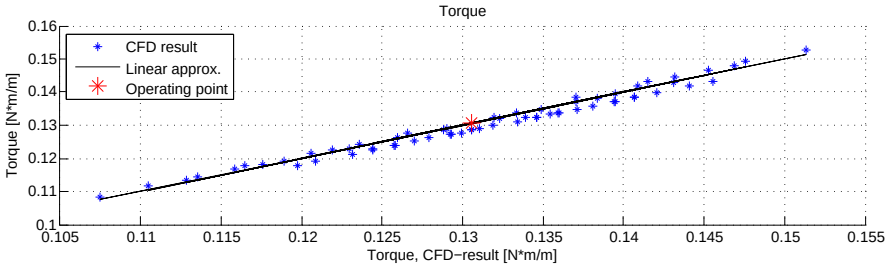

Figure 9: Torque contribution of the connecting channel: CFD results and linearized predictions, using $\Delta P = 1e5Pa$ and $\Delta\Omega = 100rad/s$, $h_{in} = 20\mu m$, $h_{out} = 50\mu m$.

4 Channel flow function: results

4.1 Pressure distribution

The next step is to apply the flow functions (equation 5) in a Reynolds-based FRB model, to see if this forms a sufficient description of the complex flow in the FRB. The coupling of the flow functions with the Reynolds-film domain was made using the Lagrange multipliers of the Reynolds flow. In the channel areas, the average cavity pressures according to equation 8 are imposed.
The Reynolds model is 1D, as the pressure is assumed to be constant over the film thickness. The model uses the parameters defined in Table 1. The outcome is compared to a 2D full FRB CFD model, which is basically the model of Section 2, but then limited to analysis of flow on the center line plane.

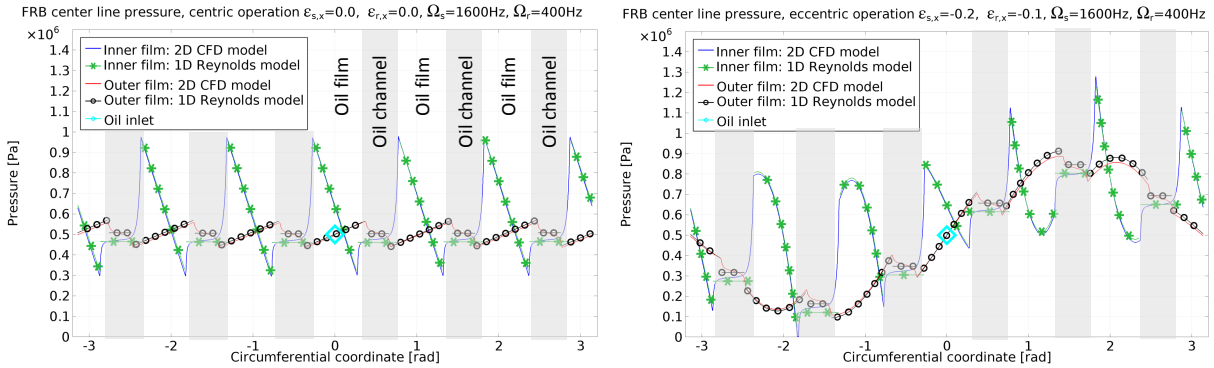

Figure 10: Center line pressure distribution in the FRB in centric (left) and eccentric (right) position. The 1D Reynolds model with the channel flow functions gives a similar prediction to the 2D CFD model.

Figure 10 shows the comparison between these models. The 1D Reynolds model, which uses the channel flow functions, is able to predict pressure profiles corresponding to the 2D CFD solution, both at centric and eccentric operation. It is important to realize that the 2D CFD model has approximately $3 \cdot 10^5$ degrees of freedom whereas the 1d Reynolds model only has $3 \cdot 10^2$ degrees of freedom.

4.2 Comparison flow function method with a pressure coupling method

The oil connecting channels can also be modeled as pure pressure equalizers, for which the pressure in the inner film over the channel area is equal to the pressure in the outer film over the channel area, see [10] for example. Figure 11 presents a comparison of this method applied to a Reynolds FRB model (in 1D) with the aforementioned methods: the 2D-CFD model and the 1D-Reynolds model using the channel flow function.

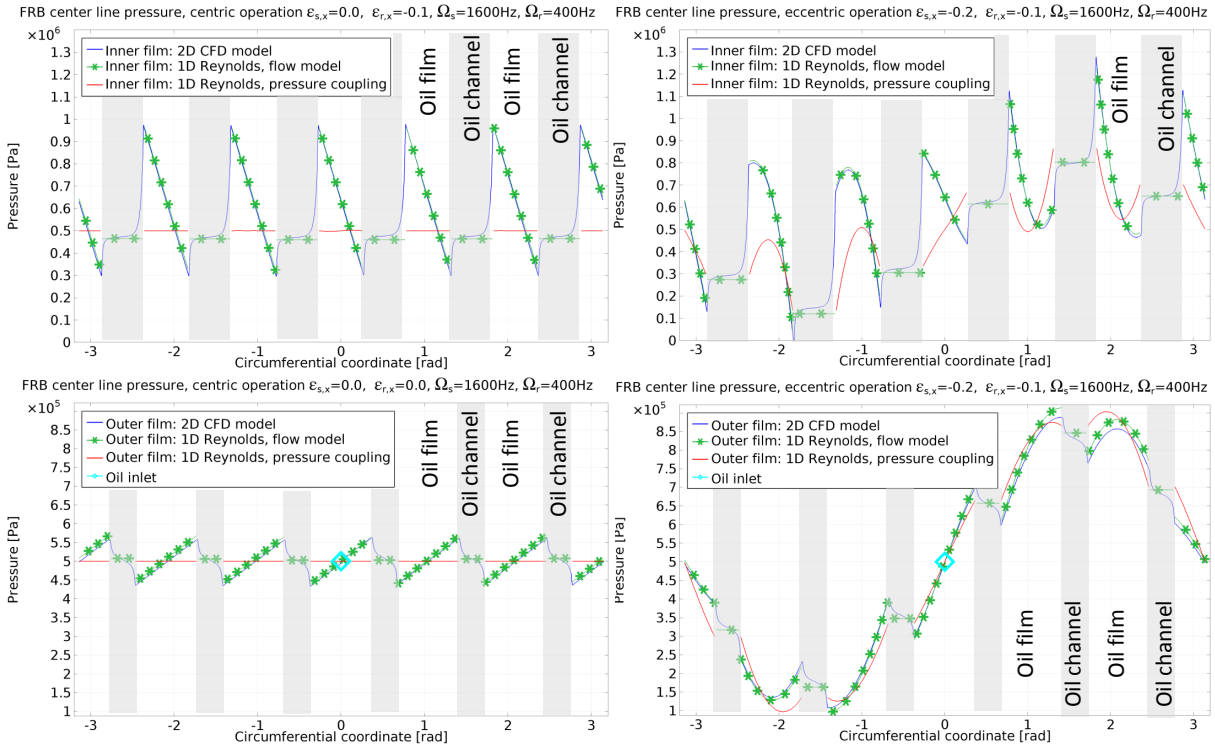

Figure 11: Center line pressure distribution in the FRB in centric (left) and eccentric (right) position. The pressure coupling method ignores the influence of the flow in the connecting channels. Hence, especially at small eccentricities, the channel flow function method presented in this study predicts pressures closer to the CFD predictions.

The pressure coupling method only includes the effect of hydrodynamic pressure buildup due to the converging and diverging sections; it ignores the internal flow in the oil connecting channels which causes the high pressure gradients at the inlet and outlet of the connecting channels. At small eccentricities ($\varepsilon < 0.3$) this method therefore gives pressure predictions which do not correspond well with the CFD pressure predictions. At larger eccentricities ($\varepsilon > 0.3$), the pressure buildup in the films of the FRB is dominated by hydrodynamic pressure buildup and therefore the pressures predicted by the pressure coupling method are similar to those predicted by the flow function method and the CFD method.

5 Conclusion

The internal flow in the oil connecting channel of a FRB is influenced by inertia and shear flow terms, causing vortices in the oil connecting channels. The shear-driven flow in the thin film sections experiences a pressure decrease when entering the channel and a pressure increase when exiting the channel, caused by both the fluid inertia as well as by the channel vortices. As the inner and outer film velocities and film thicknesses are generally not equal, there is a net difference in pressure on the side walls of the oil connecting channel, which acts as a driving torque on the ring. If this effect is neglected, the ring speed would be underestimated by $4\% - 10\%$.

A computationally inexpensive Reynolds-based model was presented, in which the channel flow is modeled as a linear combination of pressures and wall velocities surrounding the channel. Using this flow model, the effect of the connecting channels on the pressure distribution of the FRB can be included. In this way, the flow in the oil connecting channels -which was shown to have an important influence on the FRB pressure distribution- can be taken into account when performing time-transient analysis of FRBs.

Future work will be focused on extending the flow function description in axial direction. Subsequently, the model shall be used in time-transient simulations to evaluate the influence of the oil connecting channels on the behavior of a rotor on FRBs in terms of vibrations and friction losses.

REFERENCES

[1] Nguyen-Schäfer, H. (2013): *Nonlinear Rotordynamic Computations of Automotive Turbochargers using floating ring bearings at high rotor speeds*. Proceedings of SIRM, Berlin, **ABS-221**

[2] Tian, L. (2012): *Investigation into Nonlinear Dynamics of Rotor-Floating Ring Bearing Systems in Automotive Turbochargers*. Ph.D. Dissertation, University of Sussex, Falmer

[3] Boyaci, A. and Hetzler, H., Seemann, W., Proppe, C. and Wauer, J. (2008): *Analytical bifurcation analysis of a rotor supported by floating ring bearings*. Nonlinear dynamics. **57;4**, 497–507

[4] Amamou, A. and Chouchane, M. (2011): *Non-linear stability analysis of floating ring bearings using Hopf bifurcation theory*. J. of Mechanical Engineering Science. **225**

[5] Inagaki, M., Kawamoto, A., Abekura, T., Suzuki, A., Rbel, J., Starke, J. (2011): *Coupling Analysis of Dynamics and Oil Film Lubrication on Rotor - Floating Bush Bearing System*. J. of System Design and Dynamics. **5:3,461-473**

[6] Schweizer, B. (2009): *Dynamics and stability of turbocharger rotors*. Arch. Applied Mechanics. **80;9**, 1017-1043

[7] San Andrés, L. (2004): *Thermal effects on the performance of floating ring bearings for turbochargers*. J. Engineering Tribology. **218;5**, 437–450

[8] Shi, F. and Deng, D. (2011): *An Analysis for Floating Bearings in a Turbocharger*. SAE Technical Paper. **01-0375**, (2011)

[9] Porzig, D., Raetz, H. Schwarze, H., Seume, J.R., (2014): *Thermal analysis of small high-speed floating-ring journal bearings*. Int. Conf. on turbochargers and turbocharging, London

[10] E. Woschke, C. Daniel, S. Nitzschke and J. Strackeljan (2011) *Numerical run-up simulation of a turbocharger with full floating ring bearings*, The 10th International Conference on Vibration Problems 2011

[11] Perumal, D. A. (2011) *Simulation of flow in two-sided lid-driven deep cavities by finite difference method*. J. Appl. Science in thermodynamics and fluid mechanics, **6,1/2012**

[12] Comsol Multiphysics, v4.4

[13] Heckelmann, D. D. and Ettles, Mc. C. (1988) *Viscous and inertial pressure effects at the inlet to a bearing film*. Tribology Transactions, **31:1,1-5**

[14] Trippett, R.J. and Li, D.F., (1984) *High-Speed Floating-Ring Bearing Test and Analysis*. ASLE Transactions, **27:1,73-81**